Journal of Colloid and Interface Science 588 (2021) 221–231

Contents lists available at ScienceDirect

Journal of Colloid and Interface Science

journal homepage: www.elsevier.com/locate/jcis

Regular Article

Switching the solubility of electroactive ionic liquids for designing high energy supercapacitor and low potential biosensor

Michael Benjamin [a,1], Devaraj Manoj [a,1], Manickavasakam Karnan [b,1], Duraisamy Saravanakumar [a], Kathavarayan Thenmozhi [a], Katsuhiko Ariga [c,d,*], Marappan Sathish [b,c,*], Sellappan Senthilkumar [a,*]

[a] Department of Chemistry, School of Advanced Sciences, Vellore Institute of Technology (VIT), Vellore 632014, India
[b] Electrochemical Power Sources Division, CSIR-Central Electrochemical Research Institute, Karaikudi 630003, India
[c] WPI-MANA, National Institute for Materials Science (NIMS), Tsukuba 305-0044, Japan
[d] Department of Advanced Materials Science, Graduate School of Frontier Sciences, The University of Tokyo, Kashiwa 277-8561, Japan

GRAPHICAL ABSTRACT

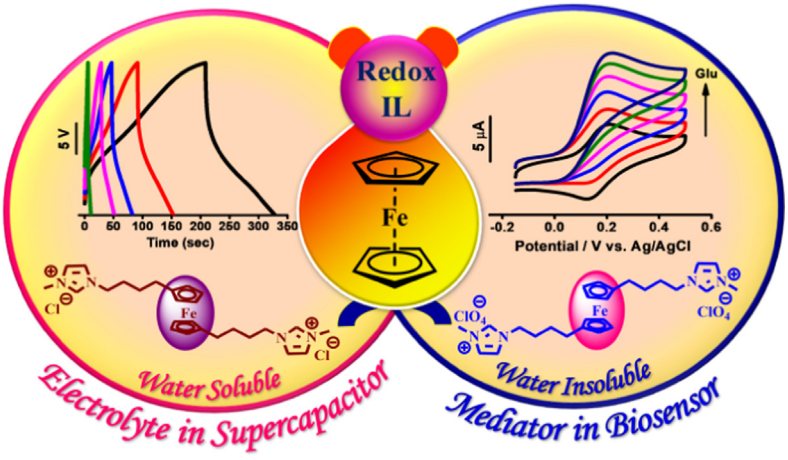

ARTICLE INFO

Article history:
Received 1 September 2020
Revised 11 December 2020
Accepted 12 December 2020
Available online 17 December 2020

Keywords:
Ionic liquids
Ferrocene
Supercapacitor
Biosensor
Energy density

ABSTRACT

Ionic liquids are regarded as one of the most prodigious materials for sustainable technological developments with superior performance and versatility. Hence, in this study, we have reported the design and synthesis of electroactive disubstituted ferrocenyl ionic liquids (Fc-ILs) with two different counter anions and demonstrated the significance of their anion tuneable physicochemical characteristics towards multifunctional electrochemical applications. The Fc-IL synthesized with chloride counter anion (Fc-Cl-IL) displays water-solubility and can be used as a redox additive in the fabrication of supercapacitor. Supercapacitor device with Fc-Cl-IL based redox electrolyte exhibits outstanding energy and power densities of 91 Wh kg^{-1} and 20.3 kW kg^{-1}, respectively. Meanwhile, ferrocenyl IL synthesized with perchlorate anion (Fc-ClO_4-IL) exhibits water-insolubility and can serve as a redox mediator towards construction of a glucose biosensor. The biosensor comprising Fc-ClO_4-IL is able to detect glucose at an exceptionally lower potential of 0.2 V, with remarkable sensitivity and selectivity. This study implies that

* Corresponding authors.
E-mail addresses: ARIGA.Katsuhiko@nims.go.jp (K. Ariga), msathish@cecri.res.in (M. Sathish), senthilkumar.s@vit.ac.in (S. Senthilkumar).
[1] Authors contributed equally to this work.

https://doi.org/10.1016/j.jcis.2020.12.033

the introduction of electroactive ILs could afford supercapacitor devices with high energy and power densities and biosensors with less detection potential.

1. Introduction

Progress in materials chemistry with the evolution of materials comprising extraordinary functional properties has led to the advancement in thrust areas of energy, environment and health science [1,2]. Amongst plethora of new materials and molecules, ferrocene (Fc) is one of the most intensively investigated organometallic molecule, whose derivatives are known to possess interesting optical, electronic, biological and redox properties [3-5]. Especially, these molecules have attracted immense interest in the development of electrochemical devices owing to the well-defined redox properties, fast electron transfer rate and highly stable redox states along with their robustness and air stability which facilitate unaltered measurements during electrochemical studies [6-8]. Accordingly, significant efforts are devoted in designing novel ferrocenyl derivatives in order to improve the compatibility of these molecules in device fabrication. Ionic liquids (ILs), a kind of organic–inorganic hybrids have pioneered as promising candidates in many pivotal areas of research including electrochemical science and technology [9,10]. ILs possess unique properties such as low vapor pressure, high chemical and thermal stability, intrinsic conductivity and wide electrochemical potential window due to which they are considered to be markedly important in electrochemistry [11-13]. Typically, ILs are composed of organic cations with organic or inorganic anions and interestingly, the physicochemical properties of these ILs can be easily tuned by suitably altering the cations and anions [14,15]. Thus, integrating the redox characteristics of ferrocene (Fc) with the flexible IL structure would result in ferrocenyl ILs (Fc-ILs) with distinguished redox behaviour and enhanced versatility, making them suitable for multifunctional applications.

Supercapacitors based on different electrode materials and electrolytes are constantly being developed with an intention of improving the energy density in terms of operating voltage and specific capacitance [16,17]. A vast effort has been devoted for the development of electrode materials [18-20], while a relatively lesser attention was paid on the electrolyte side and hence it is essential to explore the supercapacitor devices using new electrolyte systems [21,22]. Besides, aqueous electrolytes have the limitations pertaining to cell voltage while the utility of organic electrolytes is restricted due to their poor solubility and high flammability [23,24]. In order to overcome these shortcomings, IL electrolyte based supercapacitor devices have attracted foremost interest, as they could exhibit large potential window, low flammability and heat resistance [25,26]. Meanwhile, efforts were also made to increase the capacitance using suitable redox additives along with the electrolytes. The addition of redox molecules in the electrolyte offers additional pseudocapacitance (PC) along with the electrical double layer capacitance (EDLC) and thus contributing to overall enhancement in the specific capacitance [27,28]. In order to improve the supercapacitor performance, attempts were made either to utilize IL electrolytes or redox additives individually, whereas reports on redox ILs as additives or electrolytes are scarce [29]. Thus, we intend to design and synthesize a water soluble Fc-IL and to utilize it as a redox additive in the fabrication of supercapacitor with enhanced performance.

Likewise, the fabrication of both non-enzymatic and enzymatic electrochemical biosensors with promising analytical parameters is one of the pivotal areas of research in analytical and materials science [30,31]. Non-enzymatic sensors have shown outstanding sensitivity and stability, however their application in real-time detection is still challenging due to limited selectivity [32]. On the other hand, enzymatic sensors offer remarkable selectivity and reasonable sensitivity, whereas they suffer in terms of long-term stability [33]. In this regard, ILs have gained substantial attention [34-36] and their biocompatibility and ionic conductivity brand them as promising candidates for the construction of enzymatic biosensors to retain the native structure of biomolecules, resulting in augmented stability and sensitivity [37-39]. Likewise, Fc and its derivatives have shown enormous potential as mediators in electrochemical biosensors [40,41]. Coupling the redox nature of Fc with ILs would render a novel mediator/platform in electrochemical biosensing. Therefore, we sought to design a water insoluble Fc-IL and to explore its efficacy as redox mediator in enzymatic biosensing.

The physicochemical (solubility, viscosity, physical state) requirements for every electrochemical applications are different. Water insoluble redox mediators are preferred in biosensors, whereas water soluble redox additives are favoured in supercapacitor assembly. ILs being 'designer solvent' with desired physicochemical and electrochemical properties, in the present work, we aspired to synthesize ILs with tuneable/omnipotent solubility for multifunctional electrochemical applications. Limited reports are available on the synthesis of monosubstituted Fc-ILs [42,43], with substitutions on only one of the cyclopentadienyl ring and most of them are only organic soluble. Thus, we sought to synthesize disubstituted Fc-ILs in order to enhance the role of anion in altering the physicochemical characteristics of IL, whereas this task would be highly challenging with monosubstituted Fc-ILs.

Hence, in this investigation, water soluble and insoluble disubstituted Fc-ILs were synthesized by rationally tuning the anions and employed them in supercapacitor and biosensor fabrication, respectively. Initially, disubstituted ferrocenyl IL containing chloride anion (Fc-Cl-IL) was synthesized, which was obtained as water soluble liquid. This Fc-Cl-IL was used as a redox additive in aqueous electrolyte and a supercapacitor device was fabricated using bioderived activated carbon electrodes. On the other hand, water insoluble disubstituted ferrocenyl ionic liquid containing perchlorate anion (Fc-ClO_4-IL) was prepared by metathesis of Fc-Cl-IL with potassium perchlorate. This Fc-ClO_4-IL was utilized as redox mediator for the electrochemical detection of glucose using glucose oxidase (GOx) enzyme. The synthesized Fc-ILs have shown distinct performance as redox additive in supercapacitor and mediator in biosensor design.

2. Experimental

2.1. Chemicals and materials

All the reagents and solvents were used as received unless noted otherwise and all the reactions were performed with oven dried glassware. Ferrocene (98%), 1-methylimidazole (99%), 4-chlorobutyryl chloride (99%), aluminum chloride (99.99%), zinc granular (99.8%), mercury (II) chloride (98%), sodium sulphate (99%), potassium perchlorate (99.99%), polytetrafluoroethylene (PTFE), poly(vinylidene fluoride) (PVDF), deuterated chloroform ($CDCl_3$), and deuterated dimethyl sulfoxide (DMSO d_6) were

purchased from Sigma-Aldrich, India. D-glucose and glucose oxidase (from Aspergillus Niger) were received from Sisco Research Laboratories, India. Activated conducting carbon (mesoporous graphitized carbon black, 99.95%) and *N*-methyl-2-pyrrolidone (NMP, 99.5%) were purchased from Merck Chemicals, India and graphite foil (0.13 mm thick, 99.8%) was obtained from Alfa Aesar, India. Screen printed carbon electrodes (SPE) were procured from Zensor R&D, Taiwan. 0.1 M Phosphate buffer (pH 7.0) solution was prepared using Na_2HPO_4 and NaH_2PO_4 and used as a supporting electrolyte. Milli-Q water with electrical resistivity of 18.2 MΩ cm (at 25 °C) was used to prepare aqueous solutions.

2.2. Synthesis of disubstituted ferrocenyl ILs

The disubstituted ferrocenyl ILs (Fc-Cl-IL and Fc-ClO_4-IL) were synthesized using the steps mentioned in Fig. 1.

2.2.1. Synthesis of 1,1′-bis(4-chlorobutyroyl)ferrocene: 6.71 mL of 4-chlorobutyryl chloride (60 mmol) was allowed to stir with aluminum chloride (8.004 g, 60 mmol) in dry dichloromethane (25 mL) in an ice bath. After 30 min, ferrocene (3.720 g, 20 mmol) in 25 mL of dichloromethane was added dropwise to the above stirred solution over the course of 15 min (Caution: *exothermic reaction*). The reaction mixture turned dark violet and was further stirred at room temperature (RT, 30 °C) for 12 h and the reaction was monitored using thin layer chromatography. After confirming the complete reaction of Fc, the reaction mixture was poured into ice cold water and the product was extracted using dichloromethane. The organic phase was collected and dried over anhydrous sodium sulphate. Then, the solvent was removed by rotary evaporator. The residue was purified by silica column chromatography using *n*-hexane/DCM (8:2) as eluent, to obtain 1,1′-bis(4-chlorobutyroyl) ferrocene as a dark red crystalline product (1). Yield: 4.152 g; 52%. m.p.: 76 °C. IR (ATR) (ν/cm^{-1}): 3097 (Cp-H), 2924 (C-H), 1656, 1452 (C=C), 1053 (Cp), 813 (C=Cl), 474 (Cp-Fe). ^{1}H NMR (400 MHz, $CDCl_3$) δ: 2.1–2.2 (m, 2H), 2.8 (t, J = 7.2 Hz, 2H), 3.6–3.7 (t, J = 6.4 Hz, 2H), 4.5 (t, J = 2.0 Hz, 2H), 4.8 (t, J = 2.0 Hz, 2H) ppm. ^{13}C NMR (100 MHz, $CDCl_3$) δ: 26.5, 36.2, 44.7, 70.6, 73.5, 80.1, 202.1 ppm.

2.2.2. Synthesis of 1,1′-bis(4-chlorobutyl)ferrocene: Fresh Zn/Hg amalgam was prepared by stirring 12 g of Zn granules and 0.90 g of $HgCl_2$ in 10 mL of water and 0.3 mL of conc. HCl for 5 min. The amalgamated Zn was collected after discarding the aqueous supernatant and was added to a mixture of 6 mL of water and 10 mL of conc. HCl in a 100 mL RB. This mixture was continuously stirred, to which 1.970 g of 1,1′-bis(4-chlorobutyroyl)ferrocene (5 mmol) in 50 mL of toluene was added and further refluxed at 80 °C for 48 h. Conc. HCl was added to the reaction mixture in 3 mL portions at 12 h interval. The resulting reaction mixture was cooled to RT and the organic layer was separated and washed with water, followed by drying over anhydrous sodium sulphate. The crude product obtained on concentration of organic layers was purified by column chromatography on silica, using *n*-hexane as the eluent which yielded 1,1′-bis(4-chlorobutyl)ferrocene as a wine red liquid (2). Yield: 1.227 g; (66%). IR (ATR) (ν/cm^{-1}): 3084 (Cp-H), 2931 (C-H), 1637, 1442 (C=C), 1039 (Cp), 821 (C-Cl), 486 (Cp-Fe). ^{1}H NMR (400 MHz, $CDCl_3$) δ: 1.6 (m, 2H), 1.8 (m, 2H), 2.3 (t, J = 7.6 Hz, 2H), 3.5 (t, J = 6.4 Hz, 2H), 3.9 (dd, J = 1.6, 1.2 Hz, 4H) ppm. ^{13}C NMR (100 MHz, $CDCl_3$) δ: 28.4, 29.3, 32.3, 44.9, 67.9, 68.6, 88.5 ppm.

2.2.3. Synthesis of Fc-Cl-IL: The ferrocenyl ILs could be readily synthesized by nucleophilic substitution of alkylated ferrocene intermediate with methyl imidazole. 1.830 g of 1,1′-Bis(4-chlorobutyl)ferrocene (5 mmol) and 1-methylimidazole (1.231 g, 15 mmol) were taken in toluene and stirred for 72 h at 90 °C under N_2 atmosphere. The resultant solution was washed with diethyl ether several times, which afforded dimethyl-1,1′-bis(*N*-butylimidazolium) ferrocene chloride (Fc-Cl-IL) (3) as wine red viscous liquid. Yield: 2.151 g; (81%). IR (ATR) (ν/cm^{-1}): 3061 (Cp-H), 2933(C-H), 1566 (C–CC, Im$^+$), 1456 (C=C), 1166 (N$^+$-C), 1020 (Cp), 827 ($\pi_{C\text{-}H}$, Cp), 486 (Cp-Fe). ^{1}H NMR (400 MHz, DMSO d_6) δ: 1.3–1.4 (t, J = 7.2 Hz, 2H), 1.7–1.8 (t, J = 7.2 Hz, 2H), 2.2–2.3 (t, J = 7.6 Hz, 2H), 3.8 (s, 3H), 3.9 (d, J = 6.8 Hz, 4H), 4.1 (t, J = 6.4 Hz, 2H), 7.7 (s, 1H), 7.7 (s, 1H), 9.2 (s, 1H) ppm. ^{13}C NMR (100 MHz, DMSO d_6) δ: 27.7, 28.6, 29.8, 36.2, 49.0, 68.1, 68.8, 88.5, 122.7, 124.0, 137.0 ppm. HRMS (EI): m/z calculated for [M^{2+}-2Cl] $[C_{26}H_{36}FeN_4]^{2+}$ 460.4322, Found 460.4300. UV–vis {λ_{max} (DMF)/(nm)}: 432, 331 and 255. Electrical conductivity: 15.42 mS cm^{-1}.

2.2.4. Synthesis of Fc-ClO_4-IL: The perchlorate substituted ferrocenyl IL, Fc-ClO_4-IL was synthesized in good yields via anion exchange reaction of chloride containing dicationic Fc-IL with $KClO_4$. Fc-Cl-IL (1.328 g, 2.5 mmol) was dissolved in 30 mL of deionized water in RB flask and $KClO_4$ (0.718 g, 5.2 mmol) in 10 mL of water was slowly added to the solution under stirring and the stirring was continued for another 12 h at RT. The resultant yellow precipitate was collected by filtration, washed with water and dried in oven at 60 °C to obtain dimethyl-1,1′-bis(*N*-butylimidazolium)ferrocene perchlorate (Fc-ClO_4-IL) (4). Yield: 1.385 g; (84%). m.p.: 102 °C. IR (ATR) (ν/cm^{-1}): 3113 (Cp-H), 2941(C–CH), 1564 (C–CC, Im$^+$), 1456 (C=C), 1166 (N$^+$-C), 1076 and 619 (Cl-O), 1049 (Cp), 844 ($\pi_{C\text{-}H}$, Cp), 466 (Cp-Fe). ^{1}H NMR (400 MHz, DMSO d_6) δ: 1.4 (s, 2H), 1.7 (s, 2H), 2.3 (s, 2H), 3.8 (s, 3H), 3.9 (d, J = 6.8 Hz, 4H), 4.1 (s, 2H), 7.7 (s, 1H), 7.7 (s, 1H), 9.0 (s, 1H) ppm. ^{13}C NMR (100 MHz, DMSO d_6) δ: 27.2, 28.1, 29.3, 35.7, 48.6, 67.6, 68.3, 88.0, 122.2, 123.6, 136.4 ppm. HRMS (EI): m/z calculated for [M^{2+}-ClO_4] $[C_{26}H_{36}ClFe_{12}N_4O_4]^+$ 559.1610, Found 559.1699. UV–vis {λ_{max} (DMF)/(nm)}: 432, 322 and 234. Electrical conductivity: 6.64 mS cm^{-1}.

2.3. Fabrication of supercapacitor

Bio-derived activated mesoporous carbon was obtained from orange peels with high specific surface area of 2160 m^2 g^{-1} as reported earlier and the morphology, pore size and the specific surface area are presented in Figure S1 [44]. The working electrode was prepared by mixing bio-derived activated mesoporous carbon, super p-carbon black and PVDF binder in a weight ratio of 75:20:5 in NMP solvent. A homogeneous slurry was prepared using this mixture and was coated on a graphite foil (2 × 2 cm^2) as a current collector and then dried in vacuum at 80 °C for 6 h. The active material loading on the graphite foil was maintained to be ~2 mg by varying the coating thickness. In the three electrode configuration, the activated carbon coated graphite foil, Pt foil and Ag/AgCl (3 M KCl) were used as working, counter and reference electrodes, respectively. In the case of two-electrode symmetric supercapacitor, both the electrodes were coated with bio-derived carbon. The cyclic voltammetry (CV) measurements of three electrode set up were carried out in the potential range of 0.6 to −0.6 V and that of two electrode set up were performed in the range from 0 to 2.5 V using 0.1 M Fc-Cl-IL in 1 M Na_2SO_4 as the redox active electrolyte. CVs were recorded at different scan rates and the charge–discharge (CD) profiles were obtained at varying current densities. From the charge–discharge analysis, the specific capacitance (for non-Faradaic materials) and specific capacity (for Faradaic materials) of the active materials was calculated from the CD profile using eqs. (1) and (2) and also the energy and power densities were calculated using the following equations (3) and (4).

$$C_{sp} = \frac{i \times \Delta t}{\Delta V \times m} \quad (1)$$

$$Q_{sp} = \frac{I \times \Delta t}{m} \quad (2)$$

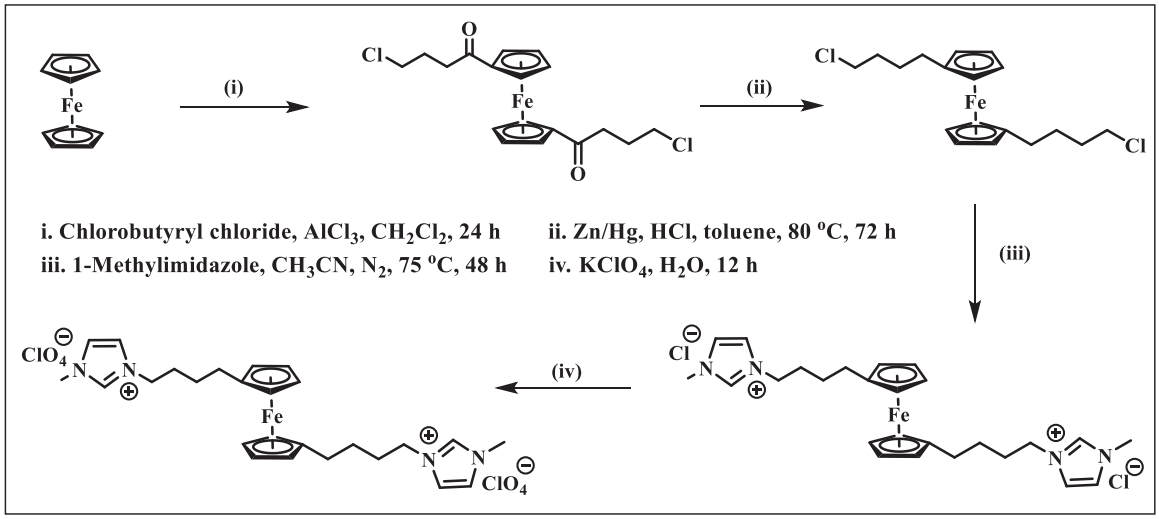

Fig. 1. Synthetic route for the preparation of ferrocenyl ionic liquids.

$$E = \frac{1}{2} C_t (\Delta V)^2 \quad (3)$$

$$P = \frac{E_t}{\Delta t} \quad (4)$$

where C_{sp} represents the specific capacitance (F/g), Q_{sp} represents the specific capacity (C/g), E is the energy density, P is the power density, i is the current density (A), Δt is the discharge time (s), m is the total active mass of the electrode materials and ΔV is the cell voltage of the device.

2.4. Fabrication of glucose biosensor

Screen printed carbon electrode (SPE) was modified using Fc-ClO_4-IL as mediator and GOx enzyme and the modified electrode was used for the electrochemical detection of glucose (Fig. 6A). Prior to modification, SPE was subjected to preanodization in 0.1 M H_2SO_4 at +2.0 V for 500 s under a constant stirring condition in N_2 atmosphere. Graphene oxide (GO) was synthesized using modified Hummer's method using the procedure reported earlier [45]. 10 μL of GO suspension (0.1 mg/mL in DMF) was dropcasted on the preanodized SPE surface and allowed to dry in air for 30 min. to obtain the GO deposited SPE (GO/SPE). After complete drying, GO was electrochemically reduced by subjecting GO/SPE to potential cycling between 0 and −1.5 V at 50 mV s^{-1} in 0.1 M phosphate buffer (pH 7.0) until a stable current profile was achieved [46]. Then, 10 μL of Fc-ClO_4-IL (2 mg/100 μL in CH_3CN) was dropped onto the surface of the electrochemically reduced GO loaded SPE (ERGO/SPE) and dried in air to obtain redox active ferrocene based IL platform (Fc-ClO_4-IL/ERGO/SPE). Subsequently, 10 μL of GOx (1 mg/100 μL in 0.1 M phosphate buffer, pH 7.0) was immobilized over Fc-ClO_4-IL/ERGO/SPE to get GOx/Fc-ClO_4-IL/ERGO/SPE and the electrode was washed with copious amount of phosphate buffer (pH 7.0) to remove the loosely bound GOx molecules. For comparison, GOx/Fc-ClO_4-IL modified SPE (GOx/Fc-ClO_4-IL/SPE) was also fabricated in the absence of ERGO using a similar procedure in order to investigate the role of ERGO in the fabricated electrochemical biosensor. The electrochemical characterization and biosensing of GOx/Fc-ClO_4-IL/SPE and GOx/Fc-ClO_4-IL/ERGO/SPE were carried out at RT with 0.1 M phosphate buffer (pH 7.0) as the supporting electrolyte. All the enzyme electrodes were stored at 5 °C when not in use.

2.5. Characterization

Melting points were determined in open capillary tubes and are uncorrected. ^{1}H and ^{13}C Nuclear magnetic resonance (NMR) spectra of the purified products were recorded in DMSO d_6 or $CDCl_3$ on a Bruker spectrometer at 400 (^{1}H) and 100 (^{13}C) MHz. Chemical shift values are given with reference to tetramethylsilane. High resolution mass spectra (HRMS) using electrospray ionization were obtained using a JEOL GC MATE II HRMS (EI). Single crystal diffraction data was collected on Bruker X8 KAPPA APEX II diffractometer using Mo Kα radiation (λ = 0.71073 Å). The crystal structure was determined and refined by direct method using SHELXL 97 and was solved by Olex 2 graphical user interface. Fourier transform infrared spectra (FTIR) were recorded on Shimadzu IR affinity-1 FTIR spectrometer using attenuated total reflectance (ATR) mode. UV–visible (UV–vis) spectra were taken using a Jasco-4100 UV–VIS-NIR-V-670 spectrophotometer.

2.6. Electrochemical measurements

The investigations on electrochemical biosensing were carried out using the CHI 760E electrochemical workstation with conventional three electrode system. A standard three electrode configuration with a bare or modified SPE as the working electrode, platinum coil as the auxiliary electrode and Ag/AgCl (3 M KCl) as reference electrode was used. All the potentials are expressed with respect to Ag/AgCl (3 M KCl). BioLogic SP-300 modular research grade potentiostat/galvanostat/FRA electrochemical workstation was used to record the CV and CD profile of the supercapacitor setup.

3. Results and discussion

3.1. Characterization of the disubstituted Fc-ILs

Disubstituted Fc-ILs have been characterized using ^{1}H and ^{13}C NMR, FTIR, UV–vis and mass spectroscopy. The NMR, UV–vis and mass spectral data of the synthesized compounds are presented in the supporting information as Figure S2-S16. The recorded ^{1}H and ^{13}C NMR spectra confirmed the proposed structures and the respective protons and carbons for all the compounds are labelled in the figures. HRMS spectra of Fc-Cl-IL and Fc-ClO_4-IL were recorded and the obtained mass matched well with that of the calculated mass for both the compounds. It was interesting to note that among the two disubstituted Fc-ILs, Fc-Cl-IL was obtained as

a liquid and Fc-ClO_4-IL was obtained as a solid. The structure of the Fc-ClO_4-IL was elucidated by single crystal X-ray diffraction as shown in Fig. 2. Crystals suitable for XRD analysis were obtained by slow evaporation of methanolic solution of Fc-ClO_4-IL at RT. The crystal data and the structure refinement along with the parametric data of the unit cells are presented in Table S1 with appropriate atom numbering and the most relevant bond lengths, bond angles and dihedral angles are given in Table S2. The crystal structure unambiguously confirmed the formation of disubstituted Fc-IL containing perchlorate anion. Crystallographic data for the structural analysis of Fc-ClO_4-IL have been deposited with the Cambridge crystallographic data center, CCDC No. 1849091 and this information may be obtained free of charge from http://www.ccdc.cam.au.uk.

The synthesized Fc-ILs were also characterized using FTIR spectra (Fig. 3A). The spectra indicated that the peak corresponding to C-H stretching of the Fc cyclic ring was observed around 3100 cm^{-1}. The band around 1470 cm^{-1} corresponds to the stretching of C=C bond found in the cyclic portion of the structure. The in-plane C-CH bending vibrations observed at 1020 cm^{-1} indicated the breathing mode of Cp ring and the band around 480 cm^{-1} is due to the stretching mode of Fe-Cp bond [47]. Further, the sharp peaks appeared around 1166 cm^{-1} for all the ILs are ascribed to the stretching bands of quaternized nitrogen (N^+C) of the imidazolium ring. Further, alkylated *N*-methyl (CH_2-N) vibrational mode observed at 1280 cm^{-1} indicated that both Fc and IL were concomitant within the molecule. The spectrum of Fc-ClO_4-IL exhibited strong and sharp bands at 1076 and 619 cm^{-1}, characteristics of the perchlorate anion which confirmed the successful metathesis of Fc-Cl-IL to Fc-ClO_4-IL.

3.2. Electrochemical behaviour of the disubstituted Fc-ILs

In order to improve the redox characteristics and also to tune the physicochemical characteristics, we have incorporated ILs to the Fc moiety and thus making them versatile and suitable for multifarious electrochemical applications. The electrochemical behaviour of the synthesized Fc-ILs has been studied by recording their CV in CH_3CN at 50 mV s^{-1} (Fig. 3B). The CV of pristine Fc was also recorded under similar conditions, which exhibited a set of redox peaks corresponding to Fc/Fc^+ redox couple with anodic (E_{pa}) and cathodic peak (E_{pc}) potentials at 0.481 and 0.385 V respectively, and a formal potential ($E°$) of 0.433 V. Upon tagging of IL, the E_{pa} and E_{pc} corresponding to Fc-Cl-IL were shifted to 0.264 and 0.189 V respectively with $E°$ of 0.226 V. Similarly, the corresponding E_{pa} and E_{pc} of Fc-ClO_4-IL were shifted to 0.215 and 0.136 V respectively, with $E°$ of 0.175 V. Thus, both the ferrocenyl ILs have advantageously demonstrated lower formal potential and good current response compared to that of unsubstituted ferrocene. These results clearly revealed that IL tagging has significantly improved the redox behaviour of the Fc moiety and making them suitable for electrochemical applications. Interestingly, the Fc-ILs exhibited different physicochemical characteristics upon changing the counter anions. Fc-Cl-IL with chloride anion was obtained as water soluble liquid and hence this IL was utilized as redox additive along with aqueous electrolyte in supercapacitor fabrication. On the other hand, the Fc-ClO_4-IL was obtained as water insoluble solid and its efficacy as mediator in glucose biosensing has been explored.

3.3. Fc-Cl-IL as redox additive in supercapacitor fabrication

The working potential of the aqueous electrolytes is limited due to the water decomposition potential. However, ILs possess high stability over wide potential window and therefore addition of ILs into the aqueous electrolyte would significantly increase the operating potential of the supercapacitor device. Thus, we have fabricated a supercapacitor device using bio-derived activated carbon based electrode and 1 M Na_2SO_4 electrolyte to which Fc-Cl-IL was added as a redox additive. The addition of Fc-Cl-IL in 1 M Na_2SO_4 electrolyte is expected to offer (i) high working potential and energy density due to the presence of IL and (ii) additional pseudocapacitance from Fc/Fc^+ redox couple. To begin with, the performance of 1 M Na_2SO_4 aqueous electrolyte was tested both in the absence and presence of Fc-Cl-IL redox additive in a three electrode system. The CVs were recorded at different scan rates ranging from 10 to 50 mV s^{-1} and a stable response was obtained from −0.6 to +0.4 V for 1 M Na_2SO_4 in the absence of Fc-Cl-IL (Fig. 4A). Further, the CD profiles were obtained at different current densities of 1, 2, 3, 4, 5 and 10 A g^{-1} which resulted in specific capacitances of 363, 287, 270, 265, 227 and 181F g^{-1} respectively (Fig. 4B).

However, upon addition of 0.1 M Fc-Cl-IL into 1 M Na_2SO_4, the redox additive electrolyte exhibited stability from −0.6 to +0.6 V (Fig. 4C) and thus it is obvious that the increase in operating voltage is mainly due to the inclusion of IL moiety into the electrolyte. Noticeably, the CD profiles obtained in 1 M Na_2SO_4 containing 0.1 M Fc-Cl-IL demonstrated very high specific capacity of 1072, 804, 656, 540, 330 and 220 C g^{-1} at 2, 3, 4, 5, 10 and 20 A g^{-1} current densities, respectively (Fig. 4D). Further, the capacitive contribution from different capacitive elements has been evaluated using Trasatti method (details are presented in supporting information). The plot of specific capacity as a function of scan rate ($\nu^{1/2}$ and $\nu^{-1/2}$) reveals the charge storing mechanism (Figure S17A-D) and the contribution of EDLC and PC were estimated. As observed from Figure S17E, the bio-derived carbon electrodes based setup has displayed a 69% and 31% contribution from EDLC (red) and PC (blue), respectively in 1 M Na_2SO_4 electrolyte. Interestingly, a dramatic change in the contribution from capacitive elements was achieved upon the addition of 0.1 M Fc-Cl-IL and it resulted in 4% and 96% contribution from EDLC and PC, respectively. Thus, the enormous increase in specific capacitance in the presence of Fc-Cl-IL is attributed to the additional faradaic capacitance derived from the redox additive.

The impressive capacitance values observed with the redox additive based electrolyte in three electrode system have motivated us towards the fabrication of a full cell in order to assess its practical utility. CVs recorded with the full cell at varying scan rates from 10 to 50 mV s^{-1}, with the 1 M Na_2SO_4 electrolyte containing 0.1 M Fc-Cl-IL, exhibited significant stability up to 2.5 V (Fig. 5A). The quasi- reversible redox peaks were observed in the CVs, which again suggested the contribution of PC from the Fc/Fc^+ redox couple. Fig. 5B shows the CD profiles obtained at different current densities of 2, 3, 4, 5 and 10 A g^{-1} and the specific capacity was calculated to be 952, 732, 560, 440 and 200 C g^{-1}, respectively. Nevertheless, the full cell constructed using the bio-derived activated carbon electrodes in 1 M Na_2SO_4 (in the absence of redox additive) has shown a very less working potential up to 1.2 V (Figure S18A) and this set up has displayed a maximum capacitance of 90 F g^{-1} only at a current density of 1 A g^{-1} (Figure S18B). Good cycle life is an essential requirement for a supercapacitor device and hence we have examined the cycle life of our supercapacitor comprising Fc-Cl-IL based redox active electrolyte by charging and discharging at a current density of 5 A g^{-1}. The supercapacitor device retained 81% of its original capacitance even after 10,000 cycles (Fig. 5C). The attained stability is mainly attributed to the Fc-Cl-IL, which could stabilize the cycle life of the cell even when it was operated at a high potential of 2.5 V. Furthermore, the Ragone plot for the fabricated device using Fc-Cl-IL based redox electrolyte has shown a high energy density of 91 Wh kg^{-1} with a much higher power density of 20.3 kW kg^{-1} (Fig. 5D). The observed specific capacitance, energy and power

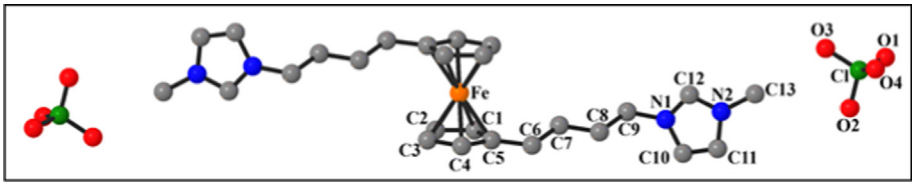

Fig. 2. Crystal structure of dimethyl-1,1́-bis(*N*-butylimidazolium)ferrocene perchlorate (Fc-ClO_4-IL).

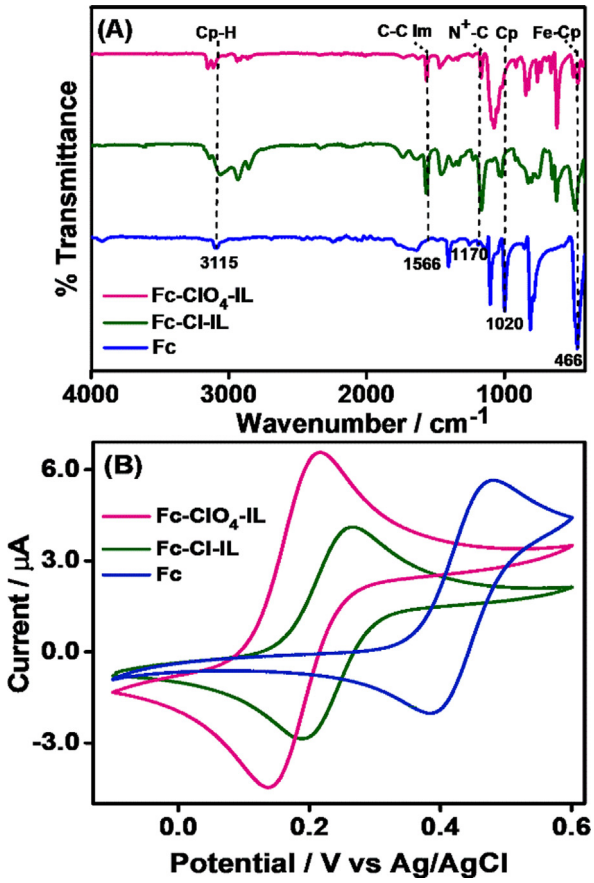

Fig. 3. (A) FTIR spectra of Fc (blue), Fc-Cl-IL (green) and Fc-ClO_4-IL (magenta) (B) CVs of 1 mM solution of Fc (blue), Fc-Cl-IL (green) and Fc-ClO_4-IL (magenta) in CH_3CN containing 0.1 M TBAP at GC electrode; scan rate: 50 mV s^{-1}. (For interpretation of the references to colour in this figure legend, the reader is referred to the web version of this article.)

densities were compared with the literature reports (Table 1). Table 1 suggests that the supercapacitor device with Fc-Cl-IL based redox electrolyte exhibits the highest energy density than that were reported in literatures, in addition to remarkable cell voltage, specific capacitance, power densities and excellent cycle life. This signifies that the Fc-Cl-IL based electrolyte could serve as a promising redox additive electrolyte for designing high performance supercapacitor device.

3.4. Fc-ClO_4-IL as mediator in glucose biosensing

After the successful demonstration of the water soluble Fc-Cl-IL as redox additive in supercapacitor fabrication, our next focus was to investigate the efficacy of the water insoluble Fc-ClO_4-IL as mediator in GOx enzyme based glucose biosensing. Thus, GOx/Fc-ClO_4-IL/ERGO/SPE modified electrode was constructed and the electrochemical behaviour was sequentially studied during the modification process by recording their CV between −0.15 and 0.50 V at a scan rate of 50 mV s^{-1} in 0.1 M phosphate buffer (pH 7.0) (Fig. 6B). As anticipated, bare SPE and ERGO deposited SPE did not show any redox peak, as they were redox inactive. GOx/Fc-ClO_4-IL/ERGO/SPE has exhibited a sharp and well resolved redox peaks with E_{pa} and E_{pc} of 0.206 and 0.129 V respectively with ΔE_p of 77 mV and E° of 0.167 V which corresponds to Fc/Fc^+ redox couple. In the meantime, the GOx/Fc-ClO_4-IL/SPE (in the absence of ERGO) depicted redox peaks with E_{pa} and E_{pc} of 0.215 and 0.112 V respectively, with ΔE_p of 103 mV and $E^\circ = 0.163$ V. The redox peaks of both GOx/Fc-ClO_4-IL/SPE and GOx/Fc-ClO_4-IL/ERGO/SPE have been observed at less formal potentials similar to solution CV (Fig. 3B), which confirmed that the electrochemistry of Fc-ClO_4-IL is well retained at the GOx modified electrode structure. A substantial increase in cathodic and anodic peak currents with less peak separation was observed for GOx/Fc-ClO_4-IL/ERGO/SPE than that of GOx/Fc-ClO_4-IL/SPE. These observations could be ascribed to the enhanced surface area offered by ERGO, and the enhanced electrical communication between Fc/Fc^+ redox center and SPE through the sp^2 conjugated network on ERGO.

In order to understand the high electrochemical activity of GOx/Fc-ClO_4-IL/ERGO/SPE, the effective surface areas of bare SPE and ERGO/SPE were estimated using Randles-Sevcik equation (5)

$$I_p = (2.69 \times 10^5)\, n^{3/2} A\, D^{1/2} C v^{1/2} \quad (5)$$

where I_p is the peak current in ampere, n is the number of electrons involved, A is the electro-active surface area of the electrode in cm^2, D is the diffusion coefficient in $cm^2\ s^{-1}$, C is the concentration in mol L^{-1} and v is scan rate in V s^{-1}. The effective surface areas of bare SPE and ERGO/SPE were found to be 0.038 and 0.072 cm^2, respectively. It is obvious that the inclusion of ERGO in the electrode setup has significantly enhanced the effective area (~2 times). This higher surface area of ERGO/SPE thereby would facilitate better immobilization of the Fc-ClO_4-IL and GOx enzyme. Further, the effect of scan rate on the GOx/Fc-ClO_4-IL/ERGO/SPE modified electrode was studied by recording CVs at different scan rates ranging from 5 to 200 mV s^{-1} in 0.1 M phosphate buffer (pH 7.0) (Figure S20). The anodic and cathodic redox peak currents increased with increasing scan rate and the linear dependence of peak currents against scan rates confirmed the surface confined process.

Investigation using electrochemical impedance spectroscopy (EIS) was also carried out in order to derive the information about the changes in the charge transfer resistance during the electrode modification. All the EIS experiments were performed in 0.1 M KCl containing 2.5 mM $[Fe(CN)_6]^{3-/4-}$ and the Nyquist plot of Z'' (imaginary component) against Z' (real component) for bare SPE, ERGO/SPE, Fc-ClO_4-IL/SPE, Fc-ClO_4-IL/ERGO/SPE, GOx/Fc-ClO_4-IL/ERGO/SPE and GOx/Fc-ClO_4-IL/SPE and the results are presented in Fig. 6C. The impedance data were fitted using Randle's circuit as shown in the inset of Fig. 6C, where R_s is electrolyte resistance, R_{ct} is charge transfer resistance, Z_w is Warburg impedance and *CPE* is constant phase element. The diameter of the semicircle represents the R_{ct} value, which is indicative of the electron transfer kinetics of the redox probe at the electrode/electrolyte interface. The Nyquist plot of bare SPE exhibited a large semicircle with an

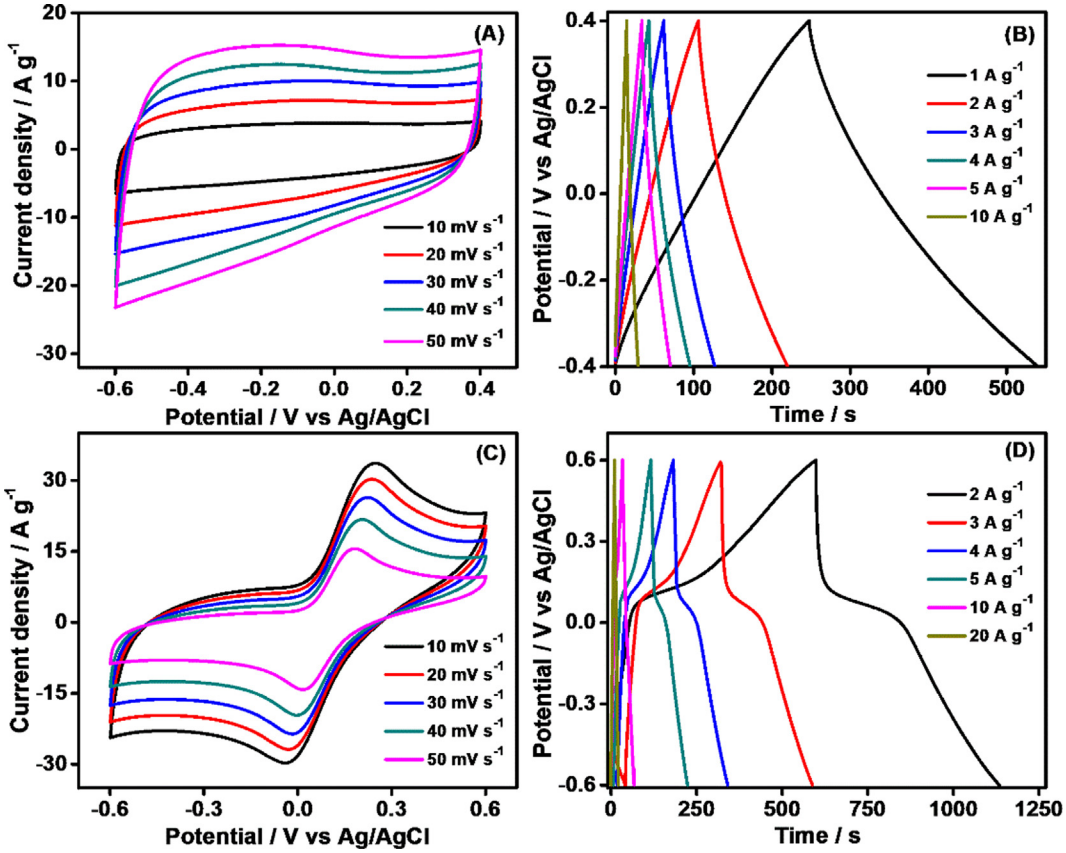

Fig. 4. Electrochemical behaviour of blank and Fc-CL-IL based redox active electrolyte in supercapacitors. (A) CVs at different scan rates and (B) CD profiles at varying current densities of bio-derived activated carbon-based electrodes in a three electrode cell with 1 M Na_2SO_4 electrolyte in the absence of Fc-Cl-IL. (C) CVs at different scan rates and (D) CD profiles at varying current densities with 1 M Na_2SO_4 electrolyte containing 0.1 M Fc-Cl-IL.

R_{ct} value of 184 Ω indicating that the electrochemical kinetics was very slow resulting in insufficient electron transfer process at the surface of bare SPE. The R_{ct} value of ERGO/SPE (107 Ω) is significantly low compared to that of bare SPE which suggested the increase in conductivity offered by ERGO. The Fc-ClO_4-IL/SPE showed a still smaller semicircle than that observed at bare SPE, indicating that the R_{ct} value (68 Ω) has been further reduced compared to bare SPE, which reveals the greater electron shuttling ability of the Fc in the IL environment. On further modification at Fc-ClO_4-IL/ERGO/SPE a reduced semicircle with substantially lower R_{ct} value (33 Ω) was observed, indicating that the charge transfer was relatively facile and also a low barrier on electron transfer has been contributed by the synergistic effect of Fc, ERGO and IL. However, with GOx/Fc-ClO_4-IL/ERGO/SPE, the impedance increased significantly to R_{ct} value of 247 Ω due to the hindrance for electron transfer through the dense protein layer of the GOx enzyme. From these EIS results, it is understood that the new platform comprising of Fc, ERGO and IL could synergistically provide good conductivity and thereby making them suitable for electrochemical biosensing.

The CV and EIS studies revealed remarkable redox behaviour and conductivity of GOx/Fc-ClO_4-IL/ERGO/SPE and thus our next step was to investigate the electrocatalytic activity of the modified electrode towards the oxidation of glucose. CVs of the bare and modified electrode were recorded in 0.1 M phosphate buffer (pH 7.0) at a scan rate of 50 mV s^{-1} (Fig. 7A) both in the absence and presence of glucose. As shown in the inset, the bare SPE did not show notable current response in the presence of glucose. However, a significant increase in the anodic peak current at a potential around 0.20 V was observed upon addition of glucose at GOx/Fc-ClO_4-IL/ERGO/SPE, depicting the electrocatalytic oxidation of glucose at the modified electrode. On successive addition of glucose, the anodic peak current increased linearly, indicative of the mediated electrocatalytic oxidation of glucose to gluconolactone at the GOx/Fc-ClO_4-IL/ERGO/SPE. During the mediated electroenzymatic process, ferrocene gets oxidized to ferrocenium ion at the electrode surface on reaching its oxidation potential. The ferrocenium ion further oxidizes the GOx($FADH_2$) to GOx(FAD) in the electrode surface. This oxidized form of GOx(FAD) is active for the oxidation of glucose to gluconolactone and consequently gets reduced to GOx ($FADH_2$). Further, the reduced GOx($FADH_2$) would be re-oxidized to GOx(FAD) form by the oxidized ferrocenium ion available at the electrode surface and this process occurs in a cyclic manner as long as the analyte is available (Eqs. (6)–(8)). This results in an enhancement in the anodic current for every addition of glucose. GOx/Fc-ClO_4-IL/ERGO/SPE modified electrode showed excellent electrocatalytic effect towards the oxidation of glucose, due to the synergistic effect of high conductivity and large electroactive surface area offered by IL and ERGO respectively along with conformational flexibility provided by GOx and fast electron shutting facilitated by Fc from the thick protein layer of the enzyme to the electrode surface in the IL background.

$$\text{Glucose} + \text{GOx(FAD)} \rightarrow \text{Gluconolactone} + \text{GOx}(FADH_2) \quad (6)$$

$$\text{GOx}(FADH_2) + Fc^{+} \rightarrow \text{GOx(FAD)} + Fc \quad (7)$$

$$Fc \iff Fc^{+} + e^{-} \quad (8)$$

Quantification of glucose was carried out by using a typical amperometric current–time response of the modified electrode at an applied potential of 0.20 V. Fig. 7B shows the amperometric

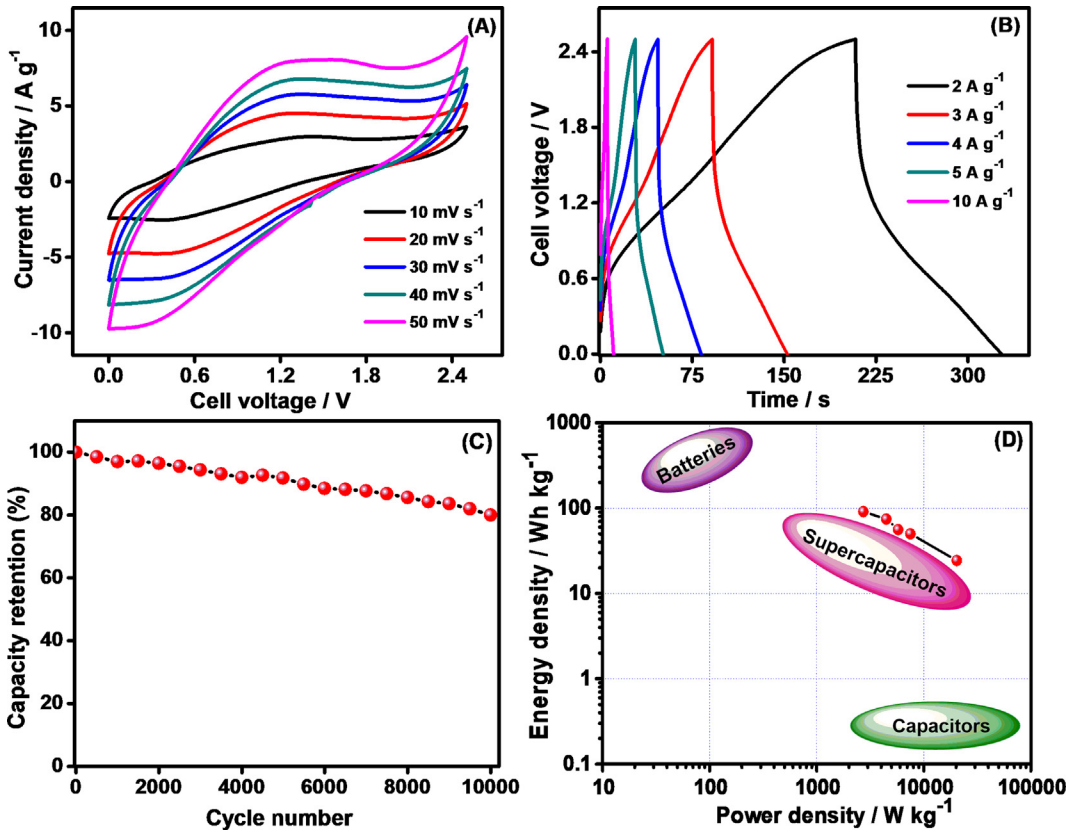

Fig. 5. Performance of Fc-Cl-IL based redox active electrolyte in supercapacitor device. (A) CVs at different scan rates and (B) CD profiles at varying current densities of bio-derived activated carbon in a two electrode cell with 1 M Na_2SO_4 electrolyte containing 0.1 M Fc-Cl-IL. (C) Long-term cyclic stability (at 2 A g^{-1}) and (D) Ragone plot of the device.

Table 1
Comparison of the performance of redox electrolytes based supercapacitors.

Electrode material	Specific capacitance (F g^{-1})	Potential window (V)	Electrolyte	Energy density (Wh kg^{-1})	Power density (kW kg^{-1})	Ref.
Nitrogen doped sheet like carbon	337	0–1.0	3,4-di hydroxy benzoic acid in H_2SO_4	14.7	1	[48]
S- Doped graphene	300	0–1.6	(HQ) in 1 M H_2SO_4	27	0.810	[49]
Biomass derived porous activated carbon	631	0–0.8	$VOSO_4$ in 1 M H_2SO_4	13.7	0.325	[50]
Bio-Carbon derived from Thespesia Populnea	1779 C g^{-1}	0–2.0	(HQ) in Na_2SO_4	76	0.994	[51]
2D carbon nanosheets	239	0–1.0	DQ + HQ in H_2SO_4	21.1	0.5	[27]
CoTe/AC	192	0–1.6	$K_4(Fe(CN)_6$ in KOH	67	0.793	[52]
Nanoporous carbon materials	636	0–1	p-phenylene diamine (ppd) in KOH	–	–	[53]
Carbon materials with high content of nitrogen and oxygen	121 & 369	0–1	Pyrocatechol and rutin in H_2SO_4	18.9 & 11.9	0.250	[54]
PANI/reduced graphene oxide(PANI-rGO) nanocomposites	409	0–1.2	Catechol in 1 M H_2SO_4	81.8	7.7	[55]
Nanoporous carbon	1499	0–1	FAS in H_2SO_4	58.70	4.5	[56]
Activated carbon	420 or 952C g^{-1}	0–2.5	Fc-Cl-IL in 1 M Na_2SO_4	91	20.3	This work

responses of GOx/Fc-ClO_4-IL/SPE and GOx/Fc-ClO_4-IL/ERGO/SPE with successive addition of varying concentration of glucose to a constantly stirred 0.1 M phosphate buffer (pH 7.0). An increase in the electrocatalytic current was observed along with well-defined stair-step as the glucose concentration was increased at a time interval of 50 s. Calibration plots were constructed by plotting the catalytic current response against the added glucose concentration (inset to Fig. 7B). GOx/Fc-ClO_4-IL/ERGO/SPE has exhibited linearity over a wide range for the detection of glucose from 0.005 to 13.8 mM with a sensitivity and detection limit of 10.9 μA mM^{-1} cm^{-2} and 1.7 μM, respectively. However, a nonlinear response with relatively poor sensitivity was obtained with GOx/Fc-ClO_4-IL/SPE.

The analytical parameters such as operating potential, linear range, detection limit and sensitivity attained using GOx/Fc-ClO_4-IL/ERGO/SPE were comparable or better than that of the recently reported Fc mediator-based glucose biosensors (Table 2), revealing the promising potentiality of the newly prepared biosensor. It is noteworthy to mention here that 0.20 V is the lowest potential reported for Fc mediated glucose biosensor. Further, the steady-

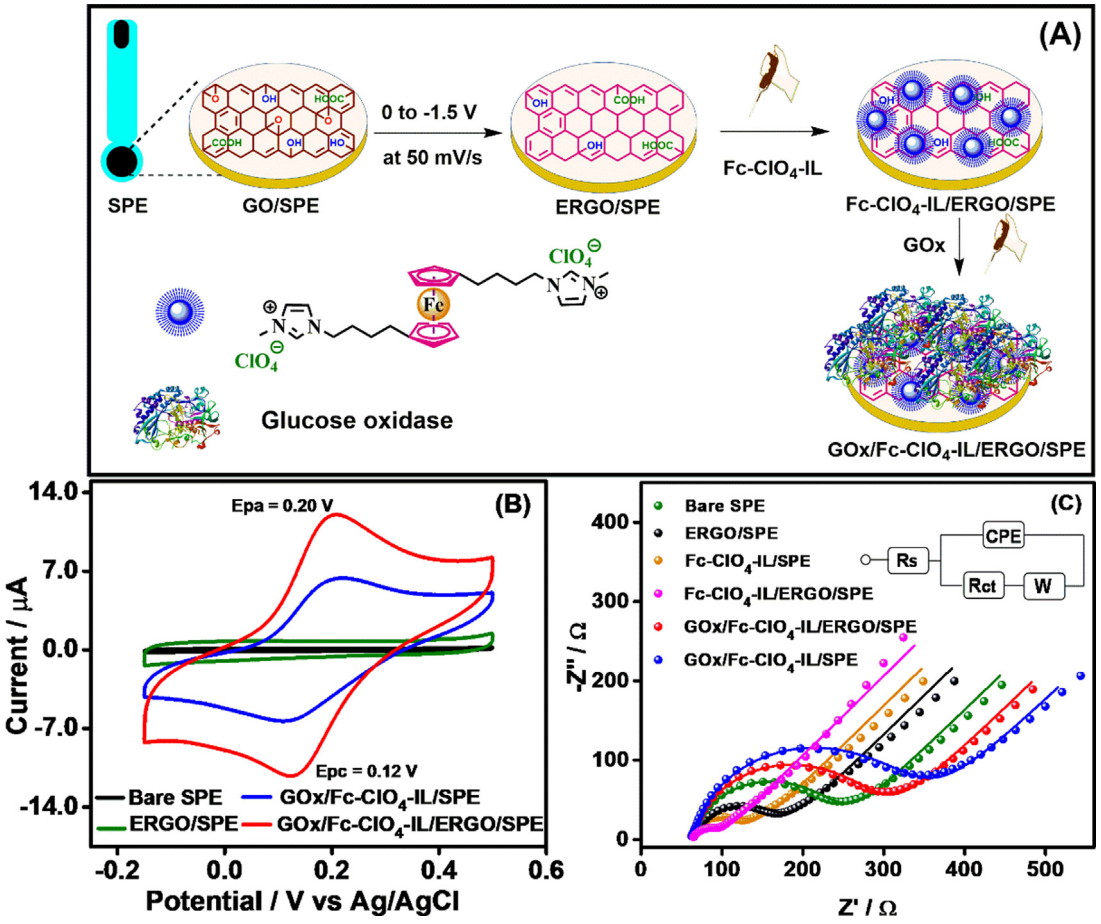

Fig. 6. (A) Schematic illustration of the steps involved in fabrication of GOx/Fc-ClO_4-IL/ERGO/SPE. (B) CVs of bare SPE (black), ERGO/SPE (green), GOx/Fc-ClO_4-IL/SPE (blue), GOx/Fc-ClO_4-IL/ERGO/SPE (red) modified electrode in 0.1 M phosphate buffer (pH 7.0) at a scan rate of 50 mV s^{-1}. (C) Nyquist plot obtained for bare SPE (green), ERGO/SPE (black), Fc-ClO_4-IL/SPE (orange), Fc-ClO_4-IL/ERGO/SPE (pink), GOx/Fc-ClO_4-IL /ERGO/SPE (red), GOx/Fc-ClO_4-IL/SPE (blue) in 0.1 M KCl containing 2.5 mM $[Fe(CN)_6]^{4-/3-}$ (For interpretation of the references to colour in this figure legend, the reader is referred to the web version of this article.)

state current for the electrocatalytic oxidation of glucose at GOx/Fc-ClO_4-IL/ERGO/SPE electrode reached 95% within 3 s for every successive injection of glucose. The instantaneous action and enhanced current response of GOx enzyme from the buried active sites was facilitated by the ample conducting platform offered by Fc-ClO_4-IL and ERGO in the biosensor setup.

The key concern and significant challenge of most biosensor design is to attain the selectivity by discriminating the common interferent species. Accordingly, the selectivity of GOx/Fc-ClO_4-IL/ERGO/SPE for glucose biosensing was tested in the presence of a series of easily oxidizable electroactive species. In the amperometric studies at an operating potential of 0.2 V in 0.1 M phosphate buffer (pH 7.0), there was a substantial enhancement of the current with steady state response during the addition of 0.1 mM glucose (Fig. 7C). The biosensor reported in this study showed no response at 0.2 V to the coexisting species such as paracetamol (PA), quercetin (QC), ascorbic acid (AA), uric acid (UA), dopamine (DA), trehalose, sucrose, fructose, L-cysteine and sodium chloride (NaCl) even at 10 times higher concentration of 1 mM as shown in Fig. 7C. This observation indicates that GOx/Fc-ClO_4-IL/ERGO/SPE exhibited excellent selectivity towards glucose detection which makes it well suitable for diagnosis of glucose even in real samples. The selectivity is ascribed to the less operating potential favoured in the ionic liquid assisted ferrocene mediated (Fc-ClO_4-IL) bioelectrocatalytic oxidation of glucose.

The operational stability of GOx/Fc-ClO_4-IL/ERGO/SPE was verified by continuous potential cycling of the fabricated biosensor in 0.1 M phosphate buffer (pH 7.0) in the potential range from −0.15 V to 0.5 V for 100 continuous cycles (Fig. 7D). The fabricated biosensor exhibited excellent stability and no obvious changes were observed in the peak current as well as peak potential in the CV curves. In addition, the long-term storage stability of the biosensor was regularly checked in the presence of glucose over a period of 30 days. We found that immobilization of GOx by the entrapment in a Fc-ClO_4-IL/ERGO/SPE was relatively stable and the modified electrode showed consistent performance without any significant change in current response during the initial 15 days of analysis and 89% of the current response was retained at the end of 30 days towards oxidation of glucose as shown in the inset Fig. 7D. This observation denoted that the fabricated biosensor retained the activity of GOx and possessed satisfactory long-term stability for glucose sensing. Furthermore, we have demonstrated the reproducibility of GOx/Fc-ClO_4-IL/ERGO/SPE by fabricating five different independently prepared electrodes by adopting similar protocol. All the five electrodes showed similar response towards 1 mM glucose with a relative standard deviation (RSD) of 1.45% revealing acceptable electrode-to-electrode reproducibility of the fabricated biosensors (inset to Fig. 7C). The biocompatible and highly conducting micro environment offered by IL and ERGO additionally favoured the suitable environment for the enzyme to maintain the native activity as well as the enhanced stability of the biosensor.

Feasibility of the fabricated biosensor towards the determination of glucose in real samples was evaluated by performing the

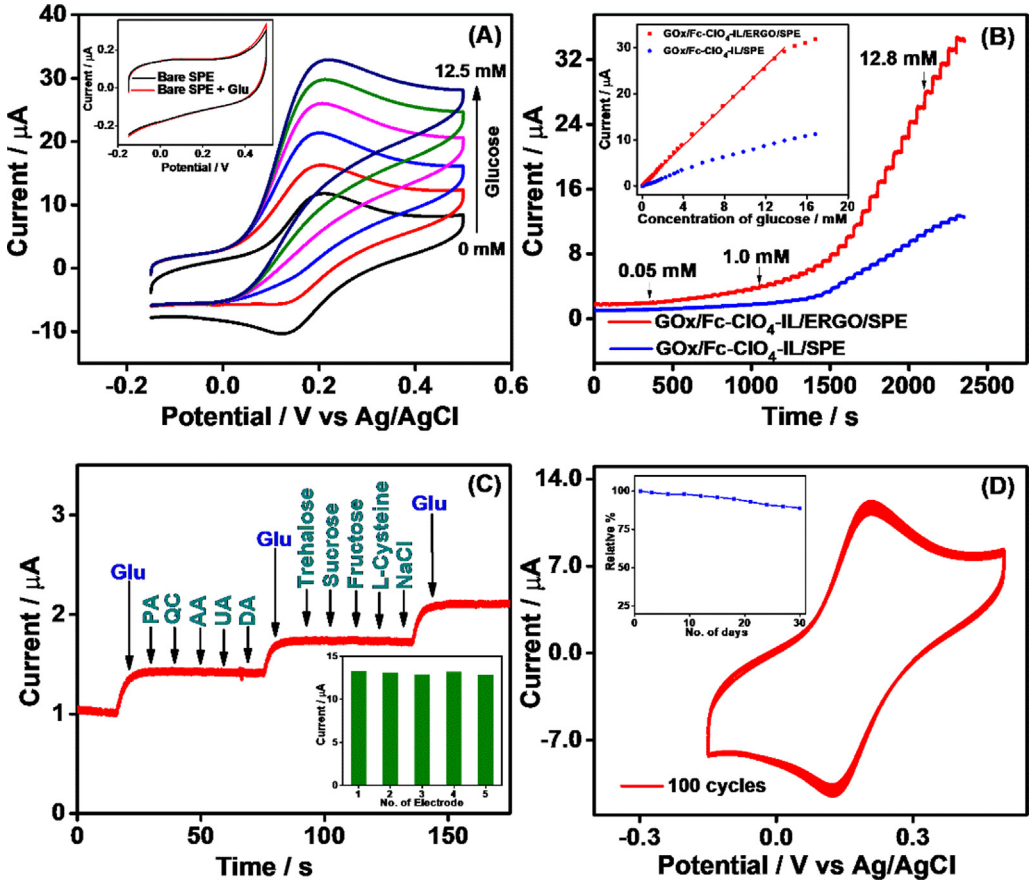

Fig. 7. (A) CVs of GOx/Fc-ClO_4-IL/ERGO/SPE with every addition of 2.5 mM glucose; Inset: CV curve of bare SPE in the absence and presence of 10 mM glucose in 0.1 M phosphate buffer (pH 7.0) at scan rate of 50 mV s^{-1} (B) Amperometric response for GOx/Fc-ClO_4-IL/SPE and GOx/Fc-ClO_4-IL/ERGO/SPE on successive additions of various concentrations of glucose into 0.1 M phosphate buffer (pH 7.0); Applied potential: +0.2 V; Stirring rate: 300 rpm; Inset: Calibration plots for the determination of glucose. (C) Interference study towards the addition of 0.15 mM glucose (Glu) and 0.5 mM of various interfering species; Inset: Demonstration of reproducibility of modified electrode and their corresponding electrocatalytic oxidation of 1 mM glucose. (D) Stability studies for GOx/Fc-ClO_4-IL/ERGO/SPE for 100 continuous cycles at a scan rate of 50 mV s^{-1} in phosphate buffer (pH 7.0); Inset: Plot of day-to-day current response for glucose biosensor.

Table 2
Comparison of the performance of glucose biosensors mediated through ferrocene and its derivatives.

Electrodes	Applied Potential (V)	Linear Range (mM)	Sensitivity (µA mM^{-1} cm^{-2})	LOD (µM)	Ref.
Fc-PNW-GOx	0.6	0.01–10	21.9	5	[57]
BPEI-Fc-GOx/SPE	0.45	0.5–4.5	27	–	[58]
Naf-GOx-ZnO-$FcC_{11}SH$/Au	0.6	0.05–1.0	27.8	20	[59]
Fc-RGOP-GOx/SPE	0.40	0.1–15.5	3.45	5	[60]
Chit-pFcAc-HAS-GOx/CP	0.41	0.1–10	0.33	–	[61]
Fc-bPEI-AuNPs-GOx/GC	0.425	0.5–10	50	40	[62]
GOx/TEOS-APTES-Fc/CS/GO	0.25	0.02–5.39	19.5	6.5	[63]
GOx/Fc/NaY	0.4	0.0008–4.0	64.5	0.2	[64]
CS-Fc/GO/GOx/GC	0.3	0.02–6.78	10	7.6	[65]
GOx/Fc-ClO_4-IL/ERGO/SPE	0.2	0.005 – 13.8	10.94	1.7	This work

Table 3
Analysis of glucose spiked in real samples (Experiments were performed in triplicate).

Sample	Spiked (mM)	Found (mM)	Recovery (%)	RSD (%)
Blood Serum	0.4	0.41	102.5	1.4
	0.6	0.6	100.0	2.0
Urine	0.5	0.49	98.0	2.1
	0.75	0.77	102.6	2.5

measurements in blood serum and urine samples. Glucose solutions of known concentrations were spiked into the electrolyte and the recoveries were calculated using amperometry, which resulted in the range from 98% to 102.6% (Figure S21) with an RSD of 1.4–2.5% (Table 3). These results illustrated that the developed low potential biosensor could selectively detect glucose even in the complex physiological conditions.

4. Conclusion

We have successfully synthesized disubstituted ferrocenyl ILs and interestingly these ILs could be readily made into either water soluble or insoluble form by suitable choice of counter anions. We have successfully demonstrated for the first time that the hydrophobicity/hydrophilicity of disubstituted Fc-ILs could be readily tuned by suitably varying the counter anions, so that they could play befitting multiple roles in electrochemistry. The ferro-

cenyl IL containing chloride anion has shown outstanding performance as a redox additive in supercapacitor fabrication. The supercapacitor device fabricated using Fc-Cl-IL based redox electrolyte has offered the highest energy density along with very high operating potential, specific capacitance, power densities and impressive cyclability [55,56]. Likewise, the water insoluble, ferrocenyl IL synthesized with perchlorate anion has inspired as an excellent mediator for glucose biosensing. The glucose biosensor thus developed has shown the lowest operating potential in addition to the remarkable linear range, sensitivity and selectivity for glucose detection with excellent long-term stability and reproducibility [63,65]. Based on the promising outcomes witnessed from the contemporary investigations, the redox active Fc-ILs unambiguously establish themselves as materials with potential advantage towards multifunctional electrochemical applications. This report on exploiting the tunability of ILs could trigger plenty of research to bring forth a variety of ILs by sensibly tuning the cation or anion for desired application.

CRediT authorship contribution statement

Michael Benjamin: Data curation, Formal analysis, Validation. **Devaraj Manoj:** Data curation, Methodology. **Manickavasakam Karnan:** Data curation, Methodology. **Duraisamy Saravanakumar:** Data curation, Validation. **Kathavarayan Thenmozhi:** . **Katsuhiko Ariga:** Conceptualization, Writing - review & editing. **Marappan Sathish:** Conceptualization, Supervision, Writing - original draft. **Sellappan Senthilkumar:** Conceptualization, Supervision, Writing - original draft.

Declaration of Competing Interest

The authors declare that they have no known competing financial interests or personal relationships that could have appeared to influence the work reported in this paper.

Acknowledgement

Council of Scientific and Industrial Research (CSIR), India (Sanction No. 01(2816)/14/EMR-II) is gratefully acknowledged for the financial support. M. S. thanks the JSPS-Bridge fellowship (BR180602) for visiting NIMS, Japan

Appendix A. Supplementary material

Supplementary data to this article can be found online at https://doi.org/10.1016/j.jcis.2020.12.033.

References

[1] S. Tadepalli, J.M. Slocik, M.K. Gupta, R.R. Naik, S. Singamaneni, Chem. Rev. 117 (2017) 12705–12763.
[2] M.-H. Sun, S.-Z. Huang, L.-H. Chen, Y. Li, X.-Y. Yang, Z.-Y. Yuan, B.-L. Su, Chem. Soc. Rev. 45 (2016) 3479–3563.
[3] H. Yang, Z. Wang, C. Li, C. Xu, J. Colloid Interface Sci. 491 (2017) 321–328.
[4] D. Xiang, G. Gao, H. Shao, H. Li, H.-L. Zhang, H.-Z. Yu, J. Phys. Chem. C. 114 (2010) 617–621.
[5] M. Patra, G. Gasser, Nat. Rev. Chem. 1 (2017) 0066.
[6] B. Fabre, Acc. Chem. Res. 43 (2010) 1509–1518.
[7] H. Li, H. Zhang, Q. Zhang, Q.-W. Zhang, D.-H. Qu, Org. Lett. 14 (2012) 5900–5903.
[8] H. Jeong, D. Kim, G. Wang, S. Park, H. Lee, K. Cho, W.-T. Hwang, M.-H. Yoon, Y.H. Jang, H. Song, D. Xiang, T. Lee, Adv. Funct. Mater. 24 (2014) 2472–2480.
[9] P. Hapiot, C. Lagrost, Chem. Rev. 108 (2008) 2238–2264.
[10] M.V. Fedorov, A.A. Kornyshev, Chem. Rev. 114 (2014) 2978–3036.
[11] R. Yan, M. Antonietti, M. Oschatz, Adv. Energy Mater. 8 (2018) 1800026.
[12] S.P. Ong, O. Andreussi, Y. Wu, N. Marzari, G. Ceder, Chem. Mater. 23 (2011) 2979–2986.
[13] M. Li, J. Yang, M. Lu, Y. Zhang, X. Bo, J. Colloid Interface Sci. 555 (2019) 449–459.
[14] J.L. Anderson, K.D. Clark, Anal. Bioanal. Chem. 410 (2018) 4565–4566.
[15] E.T. Fox, J.E.F. Weaver, W.A. Henderson, J. Phys. Chem. C 116 (2012) 5270–5274.
[16] P. Simon, Y. Gogotsi, Nat. Mater. 7 (2008) 845–854.
[17] R.X. Xu, Y.P. Zhao, G.H. Liu, J.S. Zhu, R.Y. Wang, J.P. Cao, X.Y. Wei, J. Colloid Interface Sci. 558 (2019) 211–219.
[18] Z. Tang, G. Zhang, H. Zhang, L. Wang, H. Shi, D. Wei, H. Duan, Energy Storage Mater. 10 (2018) 75–84.
[19] K. Subramani, D. Jeyakumar, M. Sathish, Phys. Chem. Chem. Phys. 16 (2014) 4952.
[20] V.K. Mariappan, K. Krishnamoorthy, P. Pazhamalai, S. Sahoo, S.J. Kim, J. Colloid Interface Sci. 556 (2019) 411–419.
[21] C. Zhong, Y. Deng, W. Hu, J. Qiao, L. Zhang, J. Zhang, Chem. Soc. Rev. 44 (2015) 7484–7539.
[22] K.O. Oyedotun, T.M. Masikhwa, S. Lindberg, A. Matic, P. Johansson, N. Manyala, Chem. Eng. J. 375 (2019) 121906.
[23] L. Hou, Z. Hu, X. Wang, L. Qiang, Y. Zhou, L. Lv, S. Li, J. Colloid Interface Sci. 540 (2019) 88–96.
[24] E. Kovalska, C. Kocabas, Mater. Today Commun. 7 (2016) 155–160.
[25] M. Karnan, K. Subramani, P.K. Srividhya, M. Sathish, Electrochim. Acta. 228 (2017) 586–596.
[26] A. Eftekhari, Energy Storage Mater. 9 (2017) 47–69.
[27] D. Xu, X.N. Sun, W. Hu, X.Y. Chen, J. Power Sources 357 (2017) 107–116.
[28] N. Yadav, N. Yadav, S.A. Hashmi, J. Power Sources 451 (2020) 227771.
[29] Y. Cui, H. Wang, N. Mao, W. Yu, J. Shi, M. Huang, W. Liu, S. Chen, X. Wang, J. Power Sources 361 (2017) 182–194.
[30] N. Wongkaew, M. Simsek, C. Griesche, A.J. Baeumner, Chem. Rev. 119 (2019) 120–194.
[31] J.-M. Jeong, M. Yang, D.S. Kim, T.J. Lee, B.G. Choi, D.H. Kim, J. Colloid Interface Sci. 506 (2017) 379–385.
[32] A.T.E. Vilian, B. Dinesh, M. Rethinasabapathy, S.-K. Hwang, C.-S. Jin, Y.S. Huh, Y.-K. Han, J. Mater. Chem. A 6 (2018) 14367–14379.
[33] A.T.E. Vilian, V. Mani, S.-M. Chen, B. Dinesh, S.-T. Huang, Ind. Eng. Chem. Res. 53 (2014) 15582–15589.
[34] M.J.A. Shiddiky, A.A.J. Torriero, Biosens. Bioelectron. 26 (2011) 1775–1787.
[35] K. Kwak, S.S. Kumar, K. Pyo, D. Lee, ACS Nano 8 (2014) 671–679.
[36] D.S. Silvester, Analyst 136 (2011) 4871.
[37] R.D. Munje, S. Muthukumar, B. Jagannath, S. Prasad, Sci. Rep. 7 (2017) 1950.
[38] D. Manoj, K. Theyagarajan, D. Saravanakumar, S. Senthilkumar, K. Thenmozhi, Biosens. Bioelectron. 103 (2018) 104–112.
[39] D. Zappi, R. Caminiti, G.M. Ingo, C. Sadun, C. Tortolini, M.L. Antonelli, Talanta 175 (2017) 566–572.
[40] X. Wang, Q. Li, J. Xu, S. Wu, T. Xiao, J. Hao, P. Yu, L. Mao, Anal. Chem. 88 (2016) 5885–5891.
[41] R.S. Dey, C.R. Raj, A.C.S. Appl, Mater. Interfaces 5 (2013) 4791–4798.
[42] H. Tahara, K. Uranaka, M. Hirano, T. Ikeda, T. Sagara, H. Murakami, A.C.S. Appl, Mater. Interfaces 11 (2019) 1–6.
[43] J. Wallauer, K. Jähme, A. Venker, P. Kübler, J. Sundermeyer, B. Roling, J. Phys. Chem. C 121 (2017) 26706–26712.
[44] K. Subramani, N. Sudhan, M. Karnan, M. Sathish, ChemistrySelect 2 (2017) 11384–11392.
[45] M. Benjamin, D. Manoj, K. Thenmozhi, P.R. Bhagat, D. Saravanakumar, S. Senthilkumar, Biosens. Bioelectron. 91 (2017) 380–387.
[46] B. Unnikrishnan, S. Palanisamy, S.M. Chen, Biosens. Bioelectron. 39 (2013) 70–75.
[47] T.P. Gryaznova, S.A. Katsyuba, V.A. Milyukov, O.G. Sinyashin, J. Organomet. Chem. 695 (2010) 2586–2595.
[48] W. Hu, D. Xu, X.N. Sun, Z.H. Xiao, X.Y. Chen, Z.J. Zhang, A.C.S. Sustain, Chem. Eng. 5 (2017) 8630–8640.
[49] M. Sandhiya, S. Suresh Balaji, M. Sathish, Energy Fuels 34 (2020) 11536–11546.
[50] S.T. Senthilkumar, R.K. Selvan, N. Ponpandian, J.S. Melo, Y.S. Lee, J. Mater. Chem. A 1 (2013) 7913.
[51] M. Karnan, S. Suresh Balaji, S. Kaipannan, A.G. Karthick Raj, S. Veeman, S. Marappan, J. Energy Storage. 32 (2020) 101939.
[52] B. Ye, C. Gong, M. Huang, Y. Tu, X. Zheng, L. Fan, J. Lin, J. Wu, RSC Adv. 8 (2018) 7997–8006.
[53] Z.J. Zhang, Z.T. Deng, Q.J. Wang, J. Electroanal. Chem. 783 (2016) 295–303.
[54] Y.F. Nie, Q. Wang, X.Y. Chen, Z.J. Zhang, J. Power Sources 320 (2016) 140–152.
[55] M.F. Mousavi, M. Hashemi, M.S. Rahmanifar, Electrochim. Acta 228 (2017) 290–298.
[56] X.N. Sun, W. Hu, D. Xu, X.Y. Chen, P. Cui, Ind. Eng. Chem. Res. 56 (2017) 2433–2443.
[57] J. Wang, D. Li, M. Yang, Y. Zhang, Anal. Methods 6 (2014) 7161–7165.
[58] J.-Y. Wang, L.-C. Chen, K.-C. Ho, ACS Appl. Mater. Interfaces 5 (2013) 7852–7861.
[59] Q. Ma, K. Nakazato, Biosens. Bioelectron. 51 (2014) 362–365.
[60] A. Halder, M. Zhang, Q. Chi, Biosens. Bioelectron. 87 (2017) 764–771.
[61] A.S. Campbell, M.F. Islam, A.J. Russell, Electrochim. Acta 248 (2017) 578–584.
[62] M.C. Dilusha Cooray, S. Sandanayake, F. Li, S.J. Langford, A.M. Bond, J. Zhang, Electroanalysis 28 (2016) 2728–2736.
[63] H. Peng, Z. Huang, Y. Zheng, W. Chen, A. Liu, X. Lin, J. Solid State Electrochem. 18 (2014) 1941–1949.
[64] J. Dong, X. Zhou, H. Zhao, J. Xu, Y. Sun, Microchim. Acta 174 (2011) 281–288.
[65] J.-D. Qiu, J. Huang, R.-P. Liang, Sens. Actuators B Chem. 160 (2011) 287–294.